

2021

Modified Canny Detector-based Active Contour for Segmentation

Radwa Alaa Salah, hussein seleem, Amira S. Ashour

Follow this and additional works at: <https://digitalcommons.aaru.edu.jo/erjeng>

Recommended Citation

Alaa Salah, hussein seleem, Amira S. Ashour, Radwa (2021) "Modified Canny Detector-based Active Contour for Segmentation," *Journal of Engineering Research*: Vol. 5: Iss. 3, Article 13.
Available at: <https://digitalcommons.aaru.edu.jo/erjeng/vol5/iss3/13>

This Article is brought to you for free and open access by Arab Journals Platform. It has been accepted for inclusion in Journal of Engineering Research by an authorized editor. The journal is hosted on [Digital Commons](#), an Elsevier platform. For more information, please contact rakan@aar.edu.jo, marah@aar.edu.jo, u.murad@aar.edu.jo.

Modified Canny Detector-based Active Contour for Medical Image Segmentation

Radwa A. Elsaywy^{1,2}, Hussein Seleem¹, Amira S. Ashour^{1,*}

¹Department of Electronics and Electrical Communications Engineering, Faculty of Engineering, Tanta University, Egypt

²Department of Electronics and Communication Engineering, Alexandria Higher Institute of Engineering & Technology (AIET), Egypt

Abstract- In the present work, an integrated modified canny detector and an active contour were proposed for automated medical image segmentation. Since the traditional canny detector (TCD) detects only the edge's pixels, which are insufficient for labelling the image, a shape feature was extracted to select the initial region of interest (RoI) as an initial mask for the active contour (AC), using a proposed modified canny detector (MCD). This procedure overcomes the drawback of the manual initialization of the mask location and shape in the traditional AC, which is sensitive to the region of interest (RoI) shape. The proposed method solves this problem by selecting the initial location and shape of the initial RoI using the MCD. Also, a post-processing stage was applied for more cleaning and smoothing the RoI. A practical computational time is achieved as the proposed system requires less than 5 minutes, which is significantly less than the required time using the traditional AC. The proposed method has complexity compared to the state-of-art methods. The assessment results showed the efficiency of the proposed approach in medical image segmentation with achieving average dice of 87.54 %.

Keywords- Segmentation; canny edge detector; shape feature extraction; region-based active contour; active contour without edges; over segmentation.

I. INTRODUCTION

The active contour (AC) model provides accurate segmentation outcomes in the different applications. There are two types of AC approaches: region-based [1,2,3] and edge-based [4,5,6] techniques. The region-based approaches are superior to the edge-based models, where the interior contours are detected automatically without using the image gradient. Chan-Vese model is the most prevalent region-based model [7], which is used in the segmentation process effectively with intensity homogeneous images. Nevertheless, it cannot segment intensity inhomogeneous images. Thus, to segment the RoI with inhomogeneous intensity, Li *et al.* [8] applied a local binary fitting model based on local image information. Local binary fitting model achieved improved performance in the segmentation accuracy compared to the piecewise smooth and piecewise constant approaches. Several studies were carried out to develop efficient methods for medical image segmentation in several applications. Kaur *et al.* [9] compared three segmentation methods, namely: active contour without edge, distance regularized level set, and localized region-based AC. The results showed the dominance of the localized region-based AC method for thyroid images segmentation in comparison with the other two methods.

Three segmentation approaches were implemented, including the active contour (level-set), feature-based classifier, and graph-cut by Wunderling *et al.* [10]. The graph-cut provided the best segmentation performance; however, it required more interaction

with the user in comparison with the other two methods. A new region-based AC model was implemented by Zhang [11], which subsumed the image's local information using the local image fitting energy function construction. Gu *et al.* [12] implemented a fractional order differentiation-based method, where the fractional order filter was specified using eight convolution masks related to the image orientation. Then, the level set method was used to the fractional-order differentiation image. In the next step, a new energy function was proposed according to the fractional order differentiation image and local image information for segmenting intensity inhomogeneity with more flexibility to the initial mask contour. Furthermore, Canny [13] implemented the traditional Canny edge detector (TCD) for designing the edge detectors of the arbitrary edge profiles. An improved canny edge detector was implemented by Bao *et al.* [14] using a scale multiplication-based approach to enhance the TCD. It multiplies the responses to improve the edge-regions for noise deletion and edge detection. On the basis of the bilateral filtering and the maximum separability of the resultant classes according to the gradient magnitudes, Jie *et al.* [15] proposed an enhanced adaptive Canny threshold. Another modified Canny edge detection approach was implemented by Biswas *et al.* [16] according to type-2 fuzzy sets which select the effective threshold values. Two adaptive double-threshold selection approaches were implemented by Rong *et al.* [17], by improving the Canny edge detection using two types of images according to the average of the image gradient and the standard deviation.

Subsequently, in the presented work, a novel model for automated AC was proposed by using a modified Canny edge detector to specify the initial mask's location, size and shape for AC model. The determination of the proposed initial mask using two steps, namely labelling the RoI using the proposed MCD for splitting each image into regions, and then, select the RoIs having the biggest area and highest intensity region using shape features. Following that, the proposed fully automated AC is implemented on the edge map image by considering the edge detection in evolving the contour. Finally, post-processing is applied to overcome the over-segmentation.

The remaining sections' organization is as follows. The proposed method of fully automated AC is explained in section II. Then, the experimental results and other studies comparisons are interpreted in section III. In section IV, the conclusion of the proposed work is highlighted.

II. METHODOLOGY

In the present method, the region-based segmentation is applied by integrating the MCD and an AC for fully automated medical image segmentation on ultrasound (US) images [10]. 16 records of 3DUS volumes including US thyroid images were used, which was divided into individual slices, to run the 2D segmentation approach. The test phase is applied on other slices different than those in the training phase, which are the central slice and ten before and after it for each

record (21 slices per record). Medical image segmentation has a significant role in several applications [18- 20]. The homogeneity within the sub-regions of the desired property is used in region-based segmentation [21], while edge-based segmentation divides the images based on the discontinuities between the sub-regions. The region-based methods have several advantages, including the ability to segment objects without edges, or with weak edges as well as generate automated interior contours. A pre-processing step was applied for de-noising using the bilateral filter to remove the speckle noise, which is the dominant noise corrupting the US images. The US images are usually bungled by noise, namely the speckle noise [22, 23]. Accordingly, the bilateral filter is employed for de-noising the US images to preserve the edges without blurring the sharp edges, destruct lines, or destroy the image's details at more speckle noise suppression. The main parameters are spatial Gaussian weighting, σ_s and intensity Gaussian weighting, σ_r . In the present work, the bilateral filter is applied with $[\sigma_s, \sigma_r] = [3, 0.1]$, where edges are lost with high values of σ_r and increasing the σ_s leads to un-blurred edges. Accordingly, the proposed method consists of three stages, namely i) region-edge detection approach using the modified Canny edge detector, ii) shape features extraction, and iii) fully automated AC followed by applying morphological operations.

A. Modified Canny Edge Detector

The proposed MCD is applied for splitting and labelling images to homogenous regions by modifying the TCD using two thresholds. This was inspired by the two main types of edges, namely pixel-based edge, and region-based edge. The TCD is pixel-based edge detection, while the proposed MCD is region-based edge, where the points at which all its neighbors have gradient magnitudes above the high threshold th_{high} are considered. In the proposed region-based edge detection method, a region of size 3×3 pixels around each edge pixel are used to have at least one pixel that have gradient magnitudes $G(x, y)$ above th_{high} to be considered as edge region. Hence, the following conditions are applied to detect the 3×3 region-based edges:

- if $G(x, y)$ is lower than the smallest threshold value, discard the edge-point or edge-region,
- else if $G(x, y)$ is above the smallest threshold value, keep the point as edge pixel.
- else if $G(x, y)$ is above th_{low} and less than th_{high} , keep the region as edges of its neighbors of region 3×3 around it if at least one pixel has gradient magnitudes above th_{high} for an edge pixel $EP(x, y)$, where the output of non-maximum step having gradient magnitude $G(x, y)$.

The edge-point and edge-region equations are formulated as:

$$E_{pixel}(x, y) = \frac{G(x, y)}{th_{high}} \quad (1)$$

$$E_{region}(x, y) = E_{pixel}(x-1, y-1) + E_{pixel}(x-1, y) + E_{pixel}(x-1, y+1) + \dots \\ E_{pixel}(x, y-1) + E_{pixel}(x, y+1) + E_{pixel}(x+1, y-1) + \dots \\ E_{pixel}(x+1, y) + E_{pixel}(x+1, y+1), \quad (2)$$

where $E_{pixel}(x, y)$ is the proposed edge map when $G(x, y)$ is above th_{high} the output is high of $E_{pixel}(x, y)$ and keep the point as edge point, and $E_{region}(x, y)$ represents the edge-region of 3×3 around a pixel, where $E_{region}(x, y)$ have high value if at least one pixel has a high value of $E_{pixel}(x, y)$. Finally, the edge map $E(x, y)$ becomes the output of this step, which is formulated as:

$$E(x, y) = E_{region}(x, y). \quad (3)$$

The edge-region is computed in the proposed MCD to generate the edge map image using the edge-region procedure to label the image regions as corresponding to an edge or not without computing the edges. The first step in the MCD is the same as the TCD as a pre-processed image is applied using a Gaussian filter for removing noise and edges are determined by calculating the gradients magnitude of the image above th_{high} . Also, only local maximum are marked as edges by the non-maximum suppression procedure. The connected edges conditions are modified as a region of size 3×3 , when surrounded by at least one pixel that has gradient magnitudes above th_{high} making this region as an edge region, unlike the TCD that generates pixel-edge. Hence, the proposed MCD detects more solid and clean edges.

B. Shape Features Extraction

For fully automated AC, a feature extraction process is conducted after MCD, where the output of the MCD includes the detection for all image regions. The feature extraction process is performed for the selection of the RoI that has the largest area and the highest intensity. The geometric shape features are calculated to identify the RoI to be the initial mask as input to automated AC. These features include the area, solidity, centroid, pixel index list, major axis length, pixel list, orientation, minor axis length, extent, eccentricity, and diameter eccentricity [24]. From the binary image of the proposed edge map $E(x, y)$, the labeled image $L(x, y)$ is created, which contains labels for the 8-connected objects found in the $E(x, y)$, which connects every two adjacent pixels of the same region along the vertical, horizontal, or diagonal direction. Afterwards, the number of pixels in each region (area properties) are calculated and evaluate the corresponding intensity values to select the largest region that has the largest number of pixels and the highest corresponding intensity (average mean), which represents the initial RoI. Generally, each region in the image can be represented by the area of the pixel shape feature of its region A , and the average intensity shape feature of its region AI as $RE(A)$, and $RE(AI)$, where, $RE(A)$ is the region of area value A , and $RE(AI)$, is the region of the average intensity value AI . The lower and upper threshold values of area and average intensity features of overall slices are $[A_L, A_H]$ and $[AI_L, AI_H]$, respectively. Thus, if the following conditions are satisfied in any

image, this region is considered the Initial RoI. These conditions are:

- if A is above A_L and less than A_H , this is called optimal area $A_{optimal}$,
- else if AI is above AI_L and less than AI_H , this is called optimal average intensity $AI_{optimal}$.

Consequently, the initial RoI selection is formulated using the following expression:

$$IROI_{Selection} = \begin{cases} RE(A_{optimal}) & A_L < A_{optimal} < A_H \\ RE(AI_{optimal}) & AI_L < AI_{optimal} < AI \end{cases} \quad (4)$$

C. Fully Automated Active Contour

The AC is considered as the most efficient image segmentation techniques. It is based on evolving contours, which identify to the various motions and object shapes in the image using one of the two main approaches, namely snake or level sets [25]. The AC methods can be classified into edge-/ region-based AC based on the force of the contour evolving. The edge-based AC relies on the image gradient to identify the location of the RoI boundary, while the image intensity of the sub-objects is considered in the region-based AC [26]. Since the US images have different intensity regions, the segmentation process is performed by applying the AC procedure as a region-based technique. Nevertheless, the drawback of the traditional AC is the necessity to manually initialize the mask location and shape, which are sensitive to the shape of RoI. So, the improvement of the traditional AC to be automated by determining the initial mask location and shape based on the RoI shape is the main contribution of the presented work.

For an image B , let Ω be a bounded open set of R^2 , which is represented by $B: \Omega \rightarrow R^2$. Afterwards, using Chan-Vese model [7], the forces W_F that control the automated initial mask evolving are evaluated, which can be expressed as follows [27] after modifying it by considering the edge map effect on the original image, $(B(b) - E(b))$:

$$W_F(CC(b), m_1, m_2) = s_1 \int_{\Omega} |(B(b) - E(b)) - m_1|^2 h(\Phi(b)) db + \dots \\ s_2 \int_{\Omega} |(B(b) - E(b)) - m_2|^2 ((B(b) - E(b)) - \dots \\ h(\Phi(b))) db + k \int_{\Omega} |\nabla h(\Phi(b))|^2 + g \int_{\Omega} h(b) db, \quad (5)$$

where $\Phi(b)$ is the Lipschitz function that can be represented by [28], also, s_1 , s_2 , k , and g are fixed constants and they are greater than zero. Also, $(B(b) - E(b))$ is the original image with edge map, thus, the contour evolution would stop at the edges. In addition, m_1 and m_2 are the mean intensity values [29] of the image inside/ outside the contour $CC(b)$ of the $(B(b) - E(b))$ image, respectively, and they are given by:

$$m_i = \frac{\int_{\Omega} (B(b) - E(b)) h(\Phi(b)) db}{\int_{\Omega} h(\Phi(b)) db}, \quad (6)$$

$$m_2 = \frac{\int_{\Omega} (B(b) - E(b)) (1 - h(\Phi(b))) db}{\int_{\Omega} (1 - h(\Phi(b))) db}, \quad (7)$$

where $CC(b)$ is the initial closed mask, which is represented by parametric curves [30], $h(\Phi(b))$ is the smooth approximate of the Heaviside function [31].

The force function $W_F(CC(b), m_1, m_2)$ is diminished using the standard gradient descent scheme [32] to drive the proposed automated initial contour to enclose the RoI by the following formula:

$$\frac{\partial \Phi}{\partial b} = \Theta(\Phi) \begin{bmatrix} (-s_1 (B(b) - E(b)) - m_1)^2 + s_2 ((B(b) - E(b)) - m_2)^2 + \dots \\ \dots \text{div} \left(\frac{\nabla \Phi}{|\nabla \Phi|^2} \right) \end{bmatrix}, \quad (8)$$

This formula refers to the force of the global image fitting to pull the contour toward the RoI based on the global image information and the contour's length, which smoothen the contour's evolving curves for the first term and second term, respectively.

Finally, a morphological procedure including dilation and erosion is used to adapt the image pixels according to its surrounded neighbouring pixels to avoid over-segmentation. The size of the pixels to be added/removed from the RoI depends to the size/shape of the used structure element. In the proposed process, the shape of structure element is square and its size is variable according to the RoI size.

D. Proposed MCD-based Active Contour

The proposed method is summarized in the following algorithm.

Algorithm: Proposed Modified Canny Edge Detector for Automated Active Contour for the Segmentation of Ultrasound Thyroid Images

Start

Input the thyroid image B

For Image slice= $1:i$

Apply bilateral filter for denoising

Apply modified Canny detector (MCD) to generate the edge map of the edge region $E(x, y)$

Compute the labelling image $L(x, y)$ from $E(x, y)$

Calculate the shape features from $L(x, y)$

Select the initial RoI that has the biggest area and the highest intensity values

Apply the proposed automated active contour model with new equations (5) and (8) with initial RoI as an initial mask, shape, and size of the AC is the initial RoI

Apply Post-Processing using morphological operations to overcome the over-segmentation |

End for

Output the segmented thyroid image

Stop

Consequently, the proposed integrated MCD with the AC includes three stages after the pre-processing stage using the bilateral filter. In the first stage, the MCD is implemented to determine the edge region in the image by generating the edge map for further use in the selection of the initial RoI as to be initial mask for AC. Afterwards, shape features extraction is applied to evaluate the area and intensity

of each region in MCD image by selecting the largest area and highest intensity region as an initial mask for AC. Finally, the fully automated AC is applied followed by applying morphological operations and shape feature extraction for a second time to perform post-processing to select the largest region and clean the image from the over-segmentation.

E. Evaluation Metrics

To evaluate the proposed automated segmentation method, several performance metrics are calculated, including the dice coefficient (DIC), Jaccard index (JACC), accuracy (ACCU), precision (PR), specificity (SPC), sensitivity (SNS), false positive rate (FPR), and false negative rate (FNR). To define these metrics, assume two images SE and GR , thus, the similarity between these two images is compared using the Dice (DIC) coefficient by the following formula [33]:

$$DIC = 2 * \frac{|SE \cap GR|}{|SE| + |GR|} = \frac{2TPR}{2TPR + FPR + FNR}, \quad (9)$$

where SE and GR are the segmented, and the ground-truth images, respectively. The operations \cap and \cup are the intersection and union operators. Also, TPR represents the true positive rate [34]. Accordingly, the JACC between these two images SE and GR is defined as the intersection between them, which can be given by:

$$JACC = \frac{|SE \cap GR|}{|SE \cup GR|} = \frac{TPR}{TPR + FPR + FNR}, \quad (10)$$

The ACCU measures the reliability of the diagnosis based on the true negative and positive predicted, which can be expressed as:

$$ACCU = \frac{TPR + TNR}{TPR + TNR + FPR + FNR}, \quad (11)$$

where TNR is the true negative rate. In predicting the RoI, the SNS indicates the TPR and the SPC indicates the TNR, which are determined, respectively, as follows:

$$SNS = \frac{TPR}{TPR + FNR}, \quad (12)$$

$$SPR = \frac{TNR}{TNR + FPR}, \quad (13)$$

The PR represents the positive detections obtained in comparison with the ground-truth, which is called positive predictive value (PPV), and can be given by:

$$PR = PPV = \frac{TPR}{TPR + FPR}, \quad (14)$$

III. EXPERIMENTAL RESULTS AND DISCUSSION

A. Results of the Proposed Segmentation Method

To highlight the superiority of the proposed MCD over the

traditional canny edge detector, Fig. 1 visualizes the results of using both procedures.

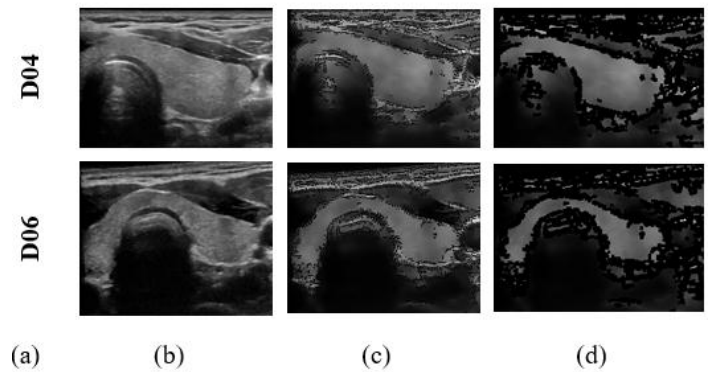


Figure 1. Edge detection results: (a) record ID of the US thyroid image, (b) original image, (c) edge detection using TCD, and (d) edge detection using the proposed MCD.

The proposed MCD labels the image and splits the image into regions for selecting the initial RoI, which is superior to using the TCD which is pixel-based method. Figure 1 shows that the edges of the MCD technique are more solid and clean compared to using the traditional Canny detector. It detects all region as a one label, unlike MCD detect each homogenous region as a different label. Consequently, the traditional Canny detector works as an edge detector only could not label the image, while the MCD could split image into sub-regions to extract shape features from each sub-region to identify the thyroid region to be an initial mask for active contour. After the edge detection, the segmentation process is applied using the AC. Since the MCD edge map image includes several edges and regions, it is followed by the shape feature extraction process to determine and specify the exact location of RoI according to the extracted features. The most relevant features are the area and intensity, which are used to specify the RoI accurately as shown in Tables 1- 3.

Table 1. The extracted features for slice 1 in the D04 record

Region label number	Average Area	Average intensity
#1	120	0.4583
#3	6409	0.4089
#16	288	0.2446
#56	275	0.2380
#87	740	0.2937
#98	196	0.2490
#99	159	0.5483

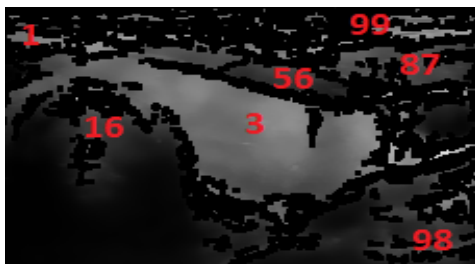
Table 2. The extracted features for slice 5 in the D04 record

Region label number	Average Area in	Average intensity
#2	5981	0.4221
#17	435	0.2644
#43	273	0.2946
#64	252	0.2452
#83	477	0.3311
#110	168	0.2641
#138	109	0.4491

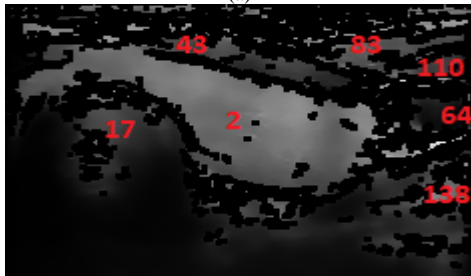
Table 3. The extracted features for slice 8 in the D04 record

Region label number	Average Area	Average intensity
2	6290	0.4080
7	483	0.2878
11	63	0.2255
18	34	0.2595
31	56	0.3832
37	584	0.2542
54	95	0.2545

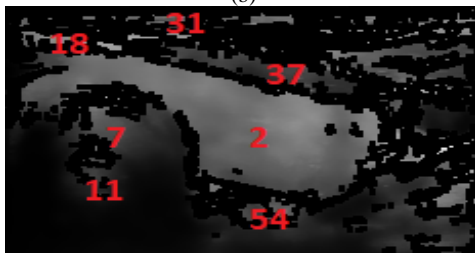
Furthermore, the proposed edge map images in the MCD for three slices with region label number for the selection of initial RoI are reported in Fig.2. Each slice is divided into multiple regions within the initial RoI hence shape feature extraction is applied on each slice for selection the initial RoI.



(a)



(b)

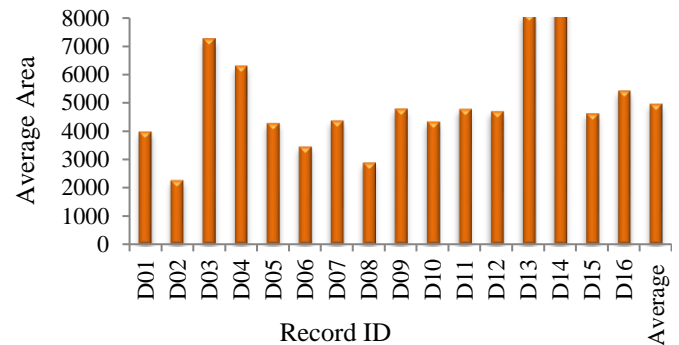
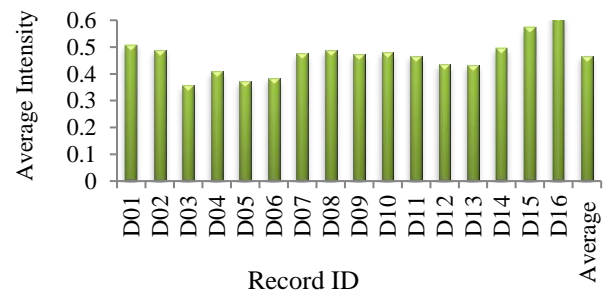


(c)

Figure 2. Edge map images of the proposed MCD showing labels' numbering of each region for selection the initial RoI for three slices of D04 record, where (a) edge map image with region label number of slice number 1, (b) edge map image with region label number of slice number 5, and (c) edge map image with region label number of slice number 8.

Figure 2 along with Tables 1- 3 illustrate the extracted features of three slices as an example for selection the initial RoI. These features include the area, solidity, centroid, pixel index list, major axis length, pixel list, orientation, minor axis length, extent, eccentricity and diameter eccentricity for each region label number. The area and average intensity feature values and their

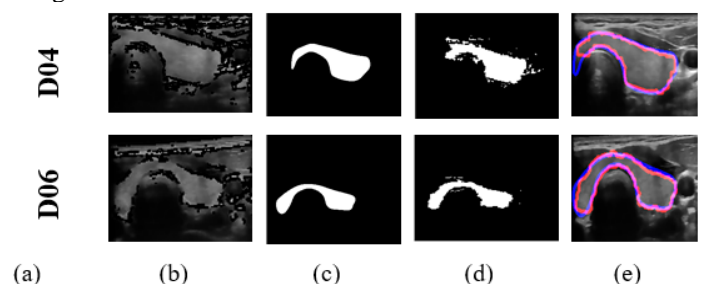
average are reported in Figs. 3 and 4, where they are the most relevant indicator to the RoI, which has the largest area and highest intensity values.

**Figure 3.** Average area of all regions in each record in the 16 records in the dataset, and their overall average value over the 16 records.**Figure 4.** Average intensity of all regions in each record in the 16 records in the dataset, and their overall average value over the 16 records.

Figures 3 and 4 demonstrated that the features' values of the average area of the overall slices in each record A_s , and average intensity AI_s of overall slices in each record and their overall average values over the sixteen records. For the RoI's overall average area, and overall average intensity values, the lower and upper threshold values of overall slices are:

$$[A_L, A_H] = [3297.22, 6617.3], \quad [AI_L, AI_H] = [0.4002, 0.53312],$$

respectively. The segmentation results of the proposed MCD-based automated AC approach are demonstrated in Fig. 5 compared to the ground-truth of the corresponding images. Fig.5 (b)-(e) showed the original image, the corresponding ground-truth, the results before post-processing stage, and the final segmented image after the morphological operations using square structure element as its shape is nearly similar to the RoI shape, respectively. In Fig.5 (e), the blue contour represents the segmented image by the proposed algorithm, and the red contour represents the corresponding ground-truth images.

**Figure 5.** Segmentation results of the proposed automated AC, where (a) dataset record

ID, (b) edge map image, (c) ground-truth image, (c) segmented image before post-processing, and (d) segmented image of proposed automated AC.

The visual results showing the accurate segmentation process by using the proposed automated AC compared to the corresponding ground-truth images was shown in Fig. 5. As shown in Figs. 6 and 7, several evaluation metrics were assessed over the dataset records for an objective assessment of the present work.

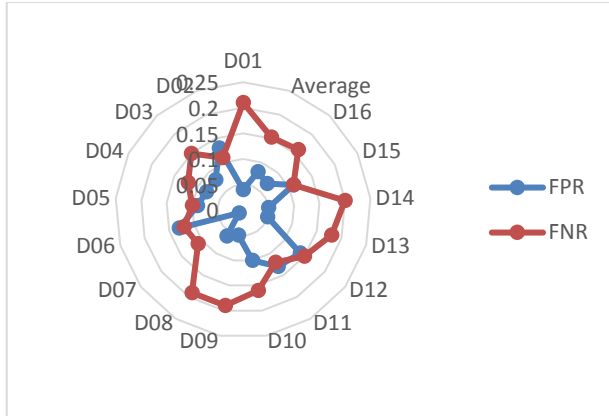


Figure 6. The FPR and FNR of the sixteen records in the dataset using the proposed automated AC method.

Figures 6 illustrates the efficiency of the proposed segmentation compared to the ground-truth images in terms of the FPR and FNR. The FPR and FNR of the proposed method are 8.757 %, and 15.37 %, respectively. Furthermore, the evaluation metrics, including the DIC, JACC, ACCU, SNS, SPC, and PR are demonstrated in Figure 7.

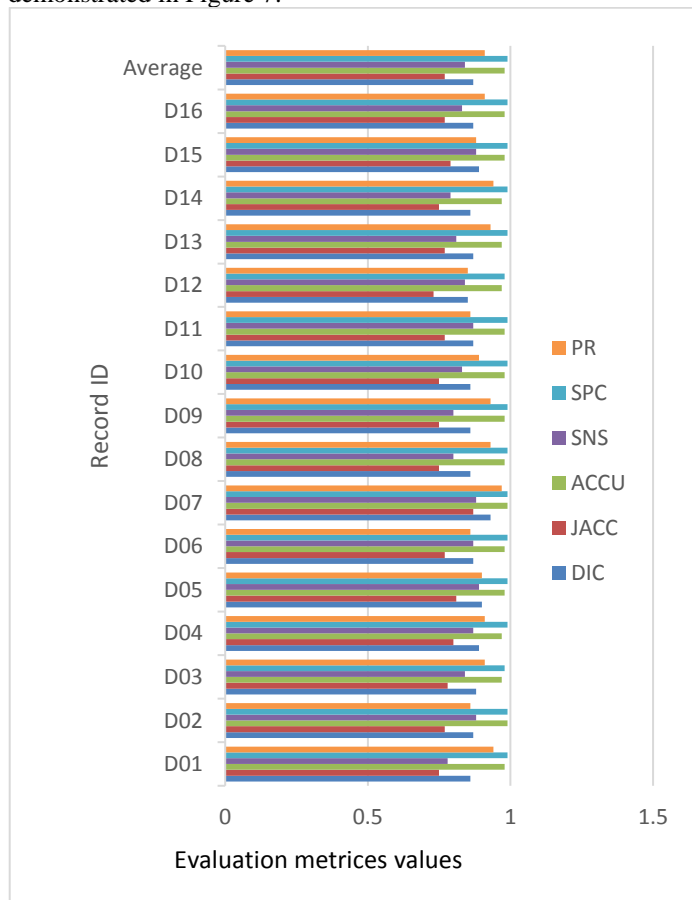


Figure 7. Evaluation metrics of the sixteen records in the dataset using the proposed automated AC method.

Figures 7 illustrated the evaluation metrics that are used for evaluating the thyroid segmentation efficiency, including the DIC, JACC, ACCU, SNS, SPC, and PR for different records in the US thyroid dataset. The proposed method achieved average DIC index of 87.54 % compared to the ground-truth images. In addition, the average values of the Jaccard index, accuracy, sensitivity, specificity, and precision are 77.87 %, 98.19 %, 84.62 %, 99.32 %, and 91.02 %, respectively.

D. Comparison with State-of-the-Art Work

The proposed automated AC method achieves improvement in the dice coefficient compared to the five segmentation methods, feedforward neural network (FNN), radial basis function (RBF) neural network, and joint classification regression (JCR), Echogenicity-based Quantization (EBQ), and Iterative Random Walks and Random Forest (IRWRF), which were reported by China *et al.* [35] on the same dataset. In addition, the comparative study included the work done by Illanes *et al.* [36], for automated thyroid segmentation of the same dataset. Table 4 reported the comparative study of the thyroid image segmentation on average over 326 images of US thyroid dataset.

Table 4. The comparative study of the average values of the evaluation metrics of the proposed method with five algorithm results reported in China *et al.* [35] and the work done by Illanes *et al.* [36].

Metrics	China <i>et al.</i> [35]					Illanes <i>et al.</i>	Proposed Method
	FNN	RBF	JCR	EBQ	IRWRF		
DIC	0.40	0.51	0.47	0.83	0.854	0.869	0.87
JACC	-	-	-	-	-	-	0.77
ACCU	-	-	-	-	-	-	0.98
SNS	0.47	0.87	0.56	0.95	0.989	0.890	0.84
SPC	0.86	0.56	0.92	0.88	0.923	0.620	0.99
PR	-	-	-	-	-	-	0.91
FPR	-	-	-	-	-	-	0.08
FNR	-	-	-	-	-	-	0.15

Table 4 established that the proposed automated AC achieves about 117.5%, 70.5%, 85.1%, 4.8%, and 2.3% improvement in the Dice index compared to the FNN, RBF, JCR, EBQ, and IRWRF, respectively, which were reported by China *et al.* [35]. Furthermore, the proposed method achieves about 0.6% improvement in the DIC over the work done by Illanes *et al.* [36]. The proposed work provides superior DIC and SP values compared to the work done in [35], and [36] on the same dataset. In addition, since the active contour is involved globally, there are many pixels indicating that there were no related pixels in the ground-truth for an expected object mask. As a result, there are many pixels are false negative leading to faintly large FNR. Consequently, the value of SNS is lower than the work done by [35, 36], but it has acceptable value.

IV. CONCLUSIONS

During the ultrasound acquisition process, the images are usually bungled by speckle noise, so bilateral filter was applied for speckle noise suppression. The present work introduced a novel automated AC model for US image segmentation based on determination the initial RoI as an initial mask to AC using the MCD and the shape features. The determination of initial RoI is performed by the MCD and shape feature extraction as the largest area, number of pixels in each region, and highest intensity value. The proposed automated active contour overcomes the problem of manual initialization of the

initial mask location and shape which are sensitive to the shape of RoI. The experiments on real frames of the used dataset showed the efficiency and superiority of the proposed automated MCD-based AC method and its ability to detect regions of different shapes, weak edges, and intensity inhomogeneity. The related work methods require more processing steps leading to more complicated segmentation methods compared to the proposed method, which has less processing steps, and less complexity. The proposed approach achieved average value of ACCU of the segmentation in the thyroid region of 98%. In addition, the average values of the DIC, JACC, SNS, PR, SPC, FNR, and FPR are 87%, 77%, 84%, 91%, 99%, 15%, and 8%, respectively. Due to the proposed fully automated AC efficiency, it is recommended to apply the presented work on real-time dataset from hospital and compare its results with using deep learning-based algorithms in the future work.

REFERENCES

- [1] Lie, M. Lysaker, X.C. Tai, A binary level set model and some application to Mumford–Shah image segmentation, *IEEE Transaction on Image Processing* 15 (2006) 1171–1181.
- [2] R. Ronfard, Region-based strategies for active contour models, *International Journal of Computer Vision* 46 (2002) 223–247.
- [3] N. Paragios, R. Deriche, Geodesic active regions and level set methods for supervised texture segmentation, *International Journal of Computer Vision* 46 (2002) 223–247.
- [4] G.P. Zhu, Sh.Q. Zhang, Q.SH. Zeng, Ch.H. Wang, Boundary-based image segmentation using binary level set method, *SPIE OE Letters* 46 (5) (2007).
- [5] V. Caselles, R. Kimmel, G. Sapiro, Geodesic active contours, *International Journal of Computer Vision* 22 (1) (1997) 61–79.
- [6] C. Xu, J.L. Prince, Snakes, shapes, and gradient vector flow, *IEEE Transaction on Image Processing* 7 (1998) 359–369.
- [7] T. F. Chan and L. A. Vese, “Active contours without edges,” *IEEE Transactions on Image Processing*, vol. 10, no. 2, pp. 266–277, 2001
- [8] Wang, L., He, L., Mishra, A., & Li, C. (2009). Active contours driven by local Gaussian distribution fitting energy. *Signal Processing*, 89(12), 2435-2447.
- [9] Kaur, J., & Jindal, A. (2012). Comparison of thyroid segmentation algorithms in ultrasound and scintigraphy images. *International Journal of Computer Applications*, 50(23).
- [10] Wunderling, T., Golla, B., Poudel, P., Arens, C., Friebe, M., & Hansen, C. (2017, February). Comparison of thyroid segmentation techniques for 3D ultrasound. In *Medical Imaging 2017: Image Processing* (Vol. 10133, p. 1013317). International Society for Optics and Photonics.
- [11] Zhang, K., Song, H., & Zhang, L. (2010). Active contours driven by local image fitting energy. *Pattern recognition*, 43(4), 1199-1206.
- [12] Gu, M., & Wang, R. (2016). Fractional differentiation-based active contour model driven by local intensity fitting energy. *Mathematical Problems in eEngineering*, 2016.
- [13] Canny, J. (1986). A computational approach to edge detection. *IEEE Transactions on pattern analysis and machine intelligence*, (6), 679-698..
- [14] Bao, P., Zhang, L., & Wu, X. (2005). Canny edge detection enhancement by scale multiplication. *IEEE transactions on pattern analysis and machine intelligence*, 27(9), 1485-1490
- [15] Jie, G., & Ning, L. (2012, March). An improved adaptive threshold canny edge detection algorithm. In *2012 International Conference on Computer Science and Electronics Engineering* (Vol. 1, pp. 164-168). IEEE.
- [16] Biswas, R., & Sil, J. (2012). An improved canny edge detection algorithm based on type-2 fuzzy sets. *Procedia Technology*, 4, 820-824.
- [17] Rong, W., Li, Z., Zhang, W., & Sun, L. (2014, August). An improved CANNY edge detection algorithm. In *2014 IEEE International Conference on Mechatronics and Automation* (pp. 577-582). IEEE
- [18] Chang, C. Y., Lei, Y. F., Tseng, C. H., & Shih, S. R. (2010). Thyroid segmentation and volume estimation in ultrasound images. *IEEE transactions on biomedical engineering*, 57(6), 1348-1357.
- [19] China, D., Illanes, A., Poudel, P., Friebe, M., Mitra, P. and Sheet, D., 2018. Anatomical structure segmentation in ultrasound volumes using cross frame belief propagating iterative random walks. *IEEE journal of biomedical and health informatics*, 23(3), pp.1110-1118.
- [20] Maheshwari, S., Pachori, R.B. and Acharya, U.R., 2016. Automated diagnosis of glaucoma using empirical wavelet transform and correntropy features extracted from fundus images. *IEEE journal of biomedical and health informatics*, 21(3), pp.803-813.
- [21] Yogamangalam, R., & Karthikeyan, B. (2013). Segmentation techniques comparison in image processing. *International Journal of Engineering and Technology (IJET)*, 5(1), 307-313.
- [22] Quistgaard, J. U. (1997). Signal acquisition and processing in medical diagnostic ultrasound. *IEEE Signal Processing Magazine*, 14(1), 67-74.
- [23] Zhang, M., & Gunturk, B. K. (2008). Multi resolution bilateral filtering for image denoising. *IEEE Transactions on image processing*, 17(12), 2324-2333.
- [24] Dharmalingham, V., & Kumar, D. (2019). A model based segmentation approach for lung segmentation from chest computer tomography images. *Multimedia Tools and Applications*, 1-26.
- [25] G.P. Zhu, Sh.Q. Zhang, Q.SH. Zeng, Ch.H. Wang, Boundary-based image segmentation using binary level set method, *SPIE OE Letters* 46 (5) (2007).
- [26] Baswaraj, D., Govardhan, A., & Premchand, P. (2012). Active contours and image segmentation: The current state of the art. *Global Journal of Computer Science and Technology*.
- [27] Maroulis, D. E., Savelonas, M. A., Iakovidis, D. K., Karkanis, S. A., & Dimitropoulos, N. (2007). Variable background active contour model for computer-aided delineation of nodules in thyroid ultrasound images. *IEEE Transactions on Information Technology in Biomedicine*, 11(5), 537-543.
- [28] Zhao, Y., Rada, L., Chen, K., Harding, S. P., & Zheng, Y. (2015). Automated vessel segmentation using infinite perimeter active contour model with hybrid region information with application to retinal images. *IEEE transactions on medical imaging*, 34(9), 1797-1807.
- [29] Wang, L., Chang, Y., Wang, H., Wu, Z., Pu, J., & Yang, X. (2017). An active contour model based on local fitted images for image segmentation. *Information sciences*, 418, 61-73.
- [30] Li, Y., & Tang, Q. (2004, August). A level set algorithm for contour tracking in medical images. In *International Workshop on Medical Imaging and Virtual Reality* (pp. 137-144). Springer, Berlin, Heidelberg.
- [31] Lv, H., Wang, Z., Fu, S., Zhang, C., Zhai, L., & Liu, X. (2017). A robust active contour segmentation based on fractional-order differentiation and fuzzy energy. *IEEE Access*, 5, 7753-7761.
- [32] G. Aubert, P. Kornprobst, *Mathematical Problems in Image Processing: Partial Differential Equations and the Calculus of Variations*, Springer, New York, 2002.
- [33] Taha, A. A., & Hanbury, A. (2015). Metrics for evaluating 3D medical image segmentation: analysis, selection, and tool. *BMC medical imaging*, 15(1), 29.
- [34] Wang, Z., Wang, E. Zhu, Y. (2020). Image segmentation evaluation: a survey of methods. *Artificial Intelligence Review*, 53(8), pp.5637-5674.
- [35] China, D., Illanes, A., Poudel, P., Friebe, M., Mitra, P., & Sheet, D. (2018). Anatomical structure segmentation in ultrasound volumes using cross frame belief propagating iterative random walks. *IEEE journal of biomedical and health informatics*, 23(3), 1110-1118.
- [36] Illanes, A., Esmaeili, N., Poudel, P., Balakrishnan, S., & Friebe, M. (2019). Parametrical modelling for texture characterization—A novel approach applied to ultrasound thyroid segmentation. *PLoS one*, 14(1).